Continuously controllable optical band gap in orthorhombic ferroelectric KNbO3-BiFeO3 ceramics

PASCUAL-GONZALEZ, Cristina, SCHILEO, Giorgio, MURAKAMI, Shunsuke, KHESRO, Amir, WANG, Dawei, REANEY, Ian and FETEIRA, Antonio <http://orcid.org/0000-0001-8151-7009>

Published version

PASCUAL-GONZALEZ, Cristina, SCHILEO, Giorgio, MURAKAMI, Shunsuke, KHESRO, Amir, WANG, Dawei, REANEY, Ian and FETEIRA, Antonio (2017). Continuously controllable optical band gap in orthorhombic ferroelectric KNbO3-BiFeO3 ceramics. Applied Physics Letters, 110 (17).

Continuously controllable optical band gap in orthorhombic ferroelectric $KNbO_3$-$BiFeO_3$ ceramics

Cristina Pascual-Gonzalez,[1] Giorgio Schileo,[2,3] Shunsuke Murakami,[2] Amir Khesro,[2] Dawei Wang,[2] Ian M. Reaney,[2] and Antonio Feteira[1]
[1]*Materials Engineering and Research Institute, Sheffield Hallam University, Howard Street, S1 1WB Sheffield, United Kingdom*
[2]*Department of Materials Science and Engineering, The University of Sheffield, Mappin Street, S1 3JD Sheffield, United Kingdom*
[3]*Dyesol UK Ltd., UMIC, 48 Grafton Street, Manchester M13 9XX, United Kingdom*

(Received 19 December 2016; accepted 10 April 2017; published online 28 April 2017)

The optical bandgap of orthorhombic ferroelectric $KNbO_3$ is shown to be continuously controllable via Bi and Fe co-substitution according to a $K_{1-x}Bi_xNb_{1-x}Fe_xO_3$ doping mechanism. The room temperature X-ray diffraction data combined with Raman spectroscopy analysis show the polar orthorhombic crystal structure to persist up to $x = 0.25$, while the bandgap narrows monotonically by 1 eV (~33%). *In-situ* Raman spectroscopy corroborates the polar nature of all compositions in the temperature range of –100 to 200 °C. The ability to control the bandgap while maintaining the spontaneous polarisation makes the $K_{1-x}Bi_xNb_{1-x}Fe_xO_3$ system interesting for photoinduced processes in a wide temperature range. [http://dx.doi.org/10.1063/1.4982600]

Coupling of light absorption in ferroelectrics (FEs) with properties such as photovoltage,[1] photostriction,[2] photoelasticity[3] and photocatalysis[4] can be exploited to create novel photoactive devices. Interestingly, the photoresponse of FEs is characterised by photovoltages that exceed several times their bandgap values.[1,5] Moreover, the internal electrical field arising from the spontaneous polarization exhibited by FEs may be employed to separate photogenerated charge carriers, enabling them to reach the surface and subsequently to interact and react with molecules in the surrounding media. In principle, photo-induced currents can also be established, provided that bandgaps of FEs are able to capture a vast range of the solar spectrum. $BiFeO_3$ with a band gap of ~2.67 eV has long been recognized to have the narrowest bandgap among robust ferroelectric perovskite oxides, while most ferroelectrics have bandgaps wider than 3 eV. These wide bandgaps limit light absorption primarily to the ultraviolet region; therefore, these materials are only able to capture ~8–20% of the solar spectrum.[6] Recently, Agarwal *et al.*[7] fabricated Si-integrated $Pt/(Bi_{0.9}Sm_{0.1})(Fe_{0.97}Hf_{0.03})O_3/LaNiO_3$ heterostructures. This doped $BiFeO_3$ thin film was reported to exhibit a band gap of 2.63 eV. Other reports[8] on double doped $BiFeO_3$ thin films exhibit similar bandgap values.

Bandgap engineering of FEs into the visible is emerging as an active research area. It has been shown that chemical doping can be strategically employed to successfully narrow the bandgap of $KNbO_3$ (KN), a well-known ferroelectric.[6,9,10] In the classic work by Shirane *et al.*,[11] the room-temperature spontaneous polarisation of single-domain KN was reported as $41 \pm 2\ \mu C/cm^2$. This large spontaneous polarisation was rationalised on the basis of the non-centrosymmetric position of Nb^{5+} cations within the NbO_6 octahedra. This distortion is driven by the hybridisation of the empty d-orbitals of Nb^{5+} with the O^{2-} p-orbitals. The relative wide optical bandgap of pure KN is also linked to the nature of the bonding between O anions and Nb cations. The large differences in electronegativity between the O and the Nb ions leads to the valence band to be formed by the 2p O states and the conduction band by the d states of the Nb transition metals sitting within the O octahedra. Hence, the excitation across the band gap in KN is essentially a charge transfer from the O 2p states at the valence band maximum (VBM) to the Nb d states at the conduction band minimum (CBM).[12] One of the strategies to narrow the band gap is by shifting up the VBM. In terms of doping, this may be achieved through substitution of Nb^{5+} in KN by lower valence Me^{3+} dopants. The repulsion between non-bonding $3d^n$ orbitals of Me^{3+} and $2p^6$ orbitals of O^{2-} may lead to a higher VBM.

Grinberg *et al.*[6] showed the bandgap of ferroelectric $(1-x)KNbO_3$-$xBaNi_{0.5}Nb_{0.5}O_{3-\delta}$ (KBNNO) ceramics to be tailored to values as low as 1.39 eV for $x = 0.10$. Nevertheless, in this system, the presence of oxygen vacancies may contribute to ~0.5 eV of the total band gap narrowing. Moreover, oxygen vacancies are detrimental to polarization switching and may also trap photogenerated charge carriers. Yu *et al.*[10] investigated $(1-x)KNbO_3$-$xBaCo_{0.5}Nb_{0.5}O_{3-\delta}$ and reported the narrowest band gap of ~2.4 eV for $x = 0.5$, but again this system contains oxygen vacancies. Recently, Pascual-Gonzalez *et al.*[9] studied bandgap engineering of $KNbO_3$ via chemical doping with a fixed 5% $Bi(Me,Yb)O_3$ (where Me = Fe or Mn) content and observed a reduction in the direct bandgap down to 2.2 eV, without having to rely on oxygen vacancies to such narrowing of the bandgap.

In this letter, the crystal structure and band structure of $(1-x)KNbO_3$-$xBiFeO_3$ (KNBF) ($0 \le x \le 0.25$) were investigated by X-ray powder diffraction combined with Raman spectroscopy and diffuse reflectance ultraviolet and visible spectroscopy (DRUV-vis). Previously,[9] it was shown that the bandgap of KN can be modified by dopants other than

transition metals, here the ability to systematically control the bandgap of $KNbO_3$ by varying the content of $BiFeO_3$ is shown. The simultaneous replacement of K^+ and Nb^{5+} by Bi^{3+} and Fe^{3+}, respectively, is expected to prevent the formation of lattice defects, such as oxygen vacancies. Nevertheless, this premise is still to be experimentally proved in future investigations, because the photovoltaic effect induced by the electromigration of oxygen vacancies is unstable.[13] The Fe^{3+} substitution for higher-valence Nb^{5+} may give rise to increased repulsion between the O 2p and Fe 3d states and thereby to a higher VBM.

KNBF ceramics were fabricated as described elsewhere[9] using the following precursor powders, K_2CO_3 (>99.0% Sigma-Aldrich), Nb_2O_5 (>99.9%, Sigma-Aldrich), Bi_2O_3 (>99.9%, Sigma-Aldrich), and Fe_2O_3 (>99.9%, Sigma-Aldrich). XRD patterns were acquired using a PANalytical diffractometer (model Empyrean) in the 2θ range 20–80, with a step size of 0.02°, and with a scan length of 600 s per step. Raman spectra were obtained with a Renishaw Raman microscope (model InVia) using a 532 nm solid state (100 mW) laser, in back-scattering geometry. Temperature-dependent Raman measurements were carried out using a Linkam stage (model THMS600). Capacitance measurements were carried out with an Agilent LCR meter (model e4980A). Finally, DRUV-vis spectra were acquired in the range 200–1600 nm using a Shimadzu UV-VIS-NIR Spectrophotometer (model UV-3600 Plus). Fine $BaSO_4$ powder was used as a non-absorbing standard. To estimate the band gaps, first the Kubelka-Munk (K-M) function given below was calculated

$$F(R) = \frac{(1-R)^2}{2R},$$

where R is the experimental reflectance referred to the $BaSO_4$ standard. Hereafter, the K-M function (or $F(R)$ curves) is considered to be proportional to the optical absorption. Hence, the absorption coefficient, α, can substituted by $F(R)$ in the Tauc equation

$$(h\nu\alpha)^n = A(h\nu - E_g) = [h\nu F(R)]^n,$$

where h is the Planck's constant, ν is the frequency of vibration, α is the absorption coefficient, E_g is the bandgap, and A is the proportional constant; for direct allowed transition, $n = 2$ and for indirect allowed transition, $n = 1/2$.

Fig. 1 shows the room-temperature XRD data for KNBF ceramics. Within the detection limits of the technique, all ceramics appear to be single-phase, as shown in Fig. 1(a). All reflections in the XRD data for undoped KN can be assigned to an orthorhombic perovskite described by the Amm2 space group. The typical peak splitting expected for a perovskite with orthorhombic crystal symmetry is clearly evident in undoped KN, but within the resolution of our measurements, only single peaks are visible for doped ceramics, as shown in Fig. 1(b); however, Raman spectroscopy provides a strong evidence that these materials are isostructural. Reflections shift slightly but systematically towards higher 2θ angles with increasing x, indicating that the co-solubility of $BiFeO_3$ and $KNbO_3$ is accompanied by a decreasing unit cell volume. The average orthorhombic crystal symmetry for the doped

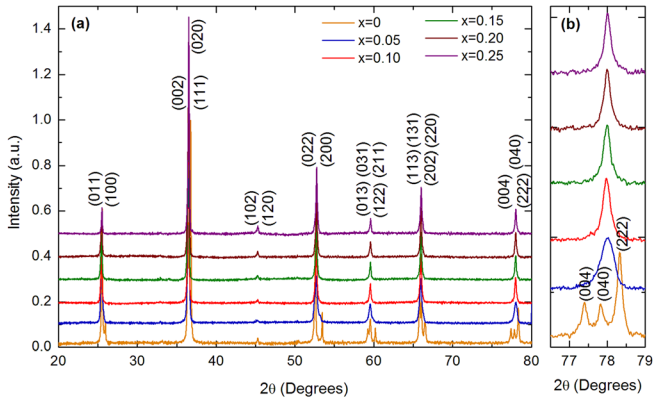

FIG. 1. Room-temperature X-ray diffraction data for KNBF ($0 \le x \le 0.25$) ceramics. (a) 2θ range 20–80 and (b) expanded view (x increases from bottom to top).

compositions is also corroborated by the Raman spectroscopy data shown in Fig. 2. The typical spectral features exhibited by the ferroelectric $KNbO_3$ orthorhombic polymorph are also visible in the Raman spectra of all doped ceramics. This spectral similarity is sufficient to simultaneously ascertain the orthorhombic crystal symmetry and the occurrence of long-range polar order in the doped materials as explained below.

From the group theory analysis, orthorhombic KN ($x = 0$) should exhibit 12 Raman active optical modes of $4A_1 + 4B_1 + 3B_2 + A_2$ symmetries, which can be separated into translational modes of isolated K^+ and internal modes of the NbO_6 octahedra. Modes in the KN Raman spectrum are labelled according to the single-crystal assignment by Quittet *et al.*[14] Hence, in the low- to mid-wavenumber region, the Raman spectrum of KN is characterised by (i) a mixed sharp mode at 192 cm^{-1}, (ii) a Fano-type interference dip at 197 cm^{-1}, (iii) a broad B_1 (TO) mode centered at 250 cm^{-1}, (iv) a B_1 (TO) at 272 cm^{-1}, (v) a sharp mode at 278 cm^{-1}, (vi) and another mode at 294 cm^{-1}. Spectral features (i), (ii), and (vi) are believed to be a fingerprint for the occurrence of long-range polar order in $KNbO_3$. The sharp mode at 192 cm^{-1} is actually a mixed mode due to B_1(TO), A_1(TO), A_1(LO), and B_2(TO) modes, while the mode at 294 cm^{-1} is due to A_1(LO) and A_1(TO), but because of the resolution limit

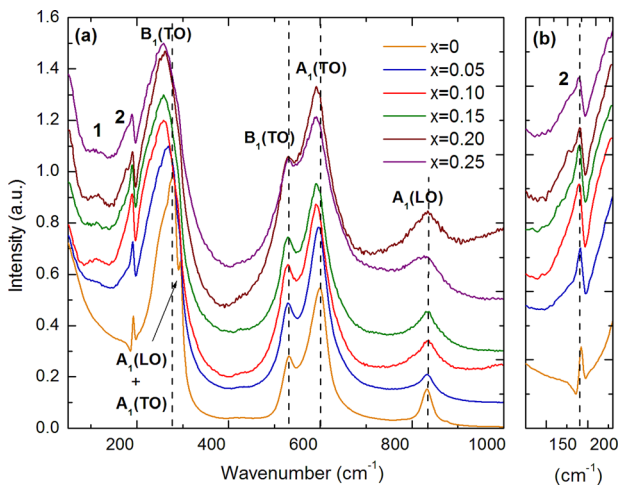

FIG. 2. Room-temperature Raman data for KNBF ($0 \le x \le 0.25$) ceramics. Dashed vertical lines are a guideline to evaluate mode shift (x increases from bottom to top).

of the instrument, they appeared merged as a single peak. The high wavenumber region (>500 cm^{-1}) of the Raman spectrum of $KNbO_3$ is characterized by a (vii) a B_1(TO) mode at ~532 cm^{-1}, (viii) a A_1(TO) mode at ~600 cm^{-1}, (ix) a low intensity A_1(LO) mode at 831 cm^{-1}.

Upon doping, new modes emerge in the low frequency regime; however, since at this stage, information on their origin is merely speculative, they are merely labelled as 1 and 2. The new mode 1 is relatively broad and appears ~110 cm^{-1}, whereas mode 2 appears as a shoulder to the sharp mixed mode at 192 cm^{-1}. The relative intensity of mode 2 appears to increase with increasing x. In the past, these modes have been associated with A-O vibrations, in particular, to nm-sized clusters rich in either Bi^{3+} or K^+ cations.[15] Finally, the A_1(LO) mode at 831 cm^{-1} appears to become broader with increasing x. This broadening may be associated with the emergence of new modes too, as previously observed, due to breathing of the octahedra, when occupied by different B cations.[9] The general broadening of the Raman modes from the doped ceramics, Fig. 2, results from increased lattice disorder, which manifests itself by the emergence of Urbach tails in the Tauc plots (Fig. 5).

Polarization, P, vs electric field, E, measurements (as will be shown elsewhere) gave unsaturated PE loops, with the exception for KN, which was considered an inconclusive response for unambiguously determining ferroelectricity. Raman spectroscopy, however, is a more reliable technique to determine the non-centrosymmetric polar character of the samples, as previously shown.[9,15] The presence of a sharp mode at 192 cm^{-1} is sufficient to prove the occurrence of long-range polar order in all compositions studied, as shown in Fig. 2(b). In a previous work,[15] monitoring of this mode was employed to show the replacement of long-range polar order by short-range polar order in (1-x)$KNbO_3$-x$BiYbO_3$ ceramics for x = 0.20 and 0.30. These two compositions exhibit so-called weak relaxor behaviour,[15] which may be regarded as a re-entrant dipole glass behaviour.[16]

The temperature dependence of the relative permittivity for KNBF (x = 0, 0.05, and 0.25) ceramics measured at 100 kHz is illustrated in Fig. 3. KN shows two clear dielectric anomalies at 394 °C and 206 °C, which can ascribed to the cubic-to-tetragonal and to the tetragonal-to-orthorhombic structural phase transitions. On the single-crystal, these transitions were reported to occur on heating at 420 °C and 220 °C, respectively.[11] This temperature discrepancy may be ascribed to the impurities present in the starting raw materials, in particular, in K_2CO_3, which has the lowest purity. Although these anomalies are also present in all doped samples, their magnitude is decreased. x = 0.25 ceramics show the highest apparent relative permittivity over the entire temperature range considered, but this may be a consequence of the fact that they have the lowest bandgap, as discussed later.

In-situ Raman spectroscopy analyses were carried out in the –100 to 200 °C temperature range in order to assert the presence of long-range polar order over a wide temperature range. For the sake of simplicity, data are only presented for KN, x = 0.05 and 0.20 at three different temperatures (–100 °C, 25 °C, and 200 °C). In Fig. 4(a), the spectra collected at –100 °C show, in the 150–300 cm^{-1} region, the spectral signature typical for the ferroelectric rhombohedral polymorph. On heating to 25 °C, the low frequency region becomes consistent with the ferroelectric orthorhombic polymorph, as shown in Fig. 4(b). Finally, at 200 °C, close to the dielectric anomalies in Fig. 3, splitting between B_1(TO) and A_1(TO) modes in the medium frequency range becomes less evident as x increases, all compositions, however, still show the features of long-range polar order. It is also worth noting that the aforementioned modes 1 and 2 are present at all temperatures. Hence, based on both permittivity measurements and Raman spectroscopy analysis, all ceramics studied exhibit dielectric anomalies associated with structural phase transitions, and their ferroelectric nature is corroborated by the presence of a Fano-type resonant dip in their Raman

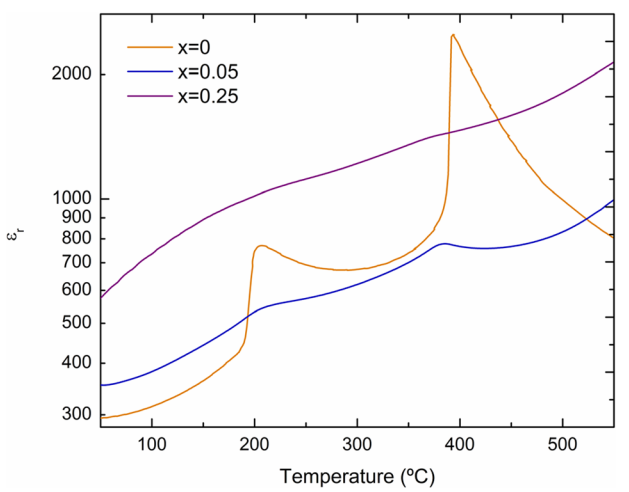

FIG. 3. Temperature dependence of ε_r for KN, x = 0.05 and x = 0.25 ceramics measured at 100 kHz.

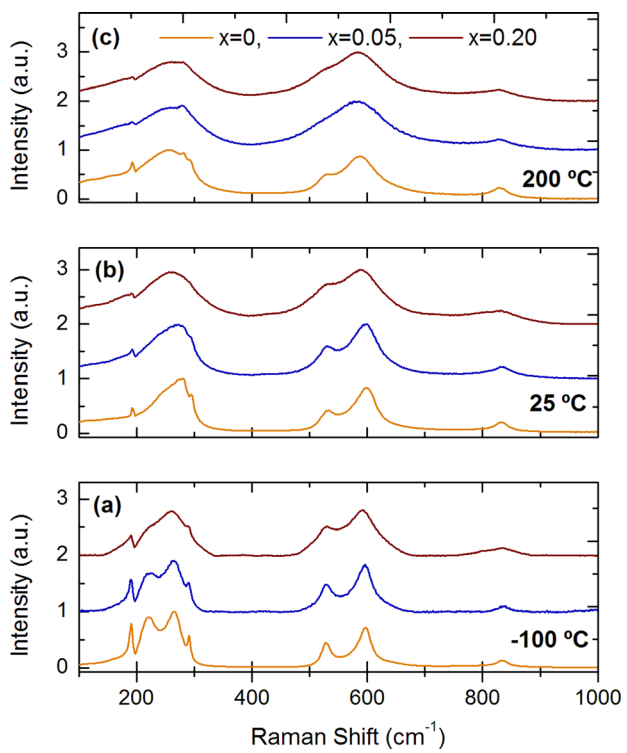

FIG. 4. *In-situ* Raman KN, x = 0.05 and x = 0.20 ceramics at (a) −100 °C, (b) 25 °C and (c) 200 °C. Bose-Einstein factor applied to data.

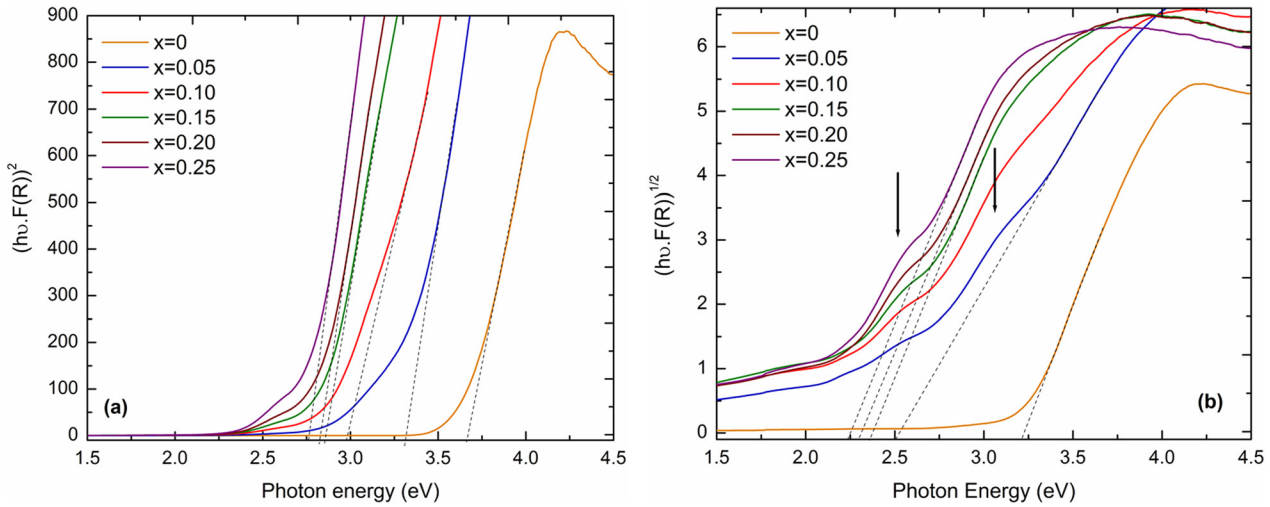

FIG. 5. Tauc plot for (a) direct and (b) indirect bandgaps for KNBF ($0 \leq x \leq 0.25$) ceramics (x increases from right to left).

spectra.[9,15] We conclude, therefore, that all studied ceramics are ferroelectric in a wide temperature range.

Finally, diffuse reflectance spectroscopy was carried out using photons with wavelengths ranging from 200 to 1600 nm. The bandgaps of KNBF ceramics were determined using the Tauc plots in Fig. 5. The bandgap energies were obtained from the intercept of the tangent line in the plot of $[h\nu F(R)]^n$ vs energy. Currently, there is no information about whether the band gap of KNBF is direct or indirect. Hence, in Fig. 5(a), the Tauc plot is constructed for $n = 2$ (direct bandgap). The value extracted for KN is 3.66 eV, a high value but within the range reported in the literature,[6] and consistent with the fact that these ceramics were able to withstand an applied electric field of 80 kV/cm. For $x = 0.05$, the value drops to ~3.22 eV; however, this still high value is inconsistent with the inability of these ceramics to withstand an electrical field as low as 5 kV/cm. Indeed, all KNBF ceramics were electrically very leaky, suggesting band gaps remarkably lower than 3 eV. Hence, in Fig. 5(b), the Tauc plot is constructed using $n = 1/2$ (indirect bandgap). The extracted bandgaps for KN and $x = 0.05$ are ~3.22 eV and ~2.5 eV, respectively, consistent with their electrical resistances. With increasing x, the bandgap narrows continuously, reaching ~2.25 eV for $x = 0.25$. We note that the apparent increase in the relative permittivity, Fig. 3, appears to follow the narrowing of the bandgaps, Fig. 5. A correlation between the dielectric response and optical behaviour of several other $KNbO_3$-based solid solutions is reported elsewhere.[6,17] The Tauc plot in Fig. 5(b) is marked by photoresponsive phenomena other than the direct charge transfer between O and Nb atoms, i.e., across the bandgap. Around 2.5 eV, there is a clear shoulder, present in all doped materials, whose magnitude increases with increasing x. The optical absorption spectra of Fe^{3+} containing substances are known to exhibit three types of electronic transitions, namely, Fe^{3+} ligand field transitions or the d-d transitions, ligand to metal charge transfer transitions, and pair excitations resulting from the simultaneous excitation of two neighbouring Fe^{3+} that are magnetically coupled. Bukert *et al.*[18] carried out an optical spectroscopy study in $BiFeO_3$ and observed three well-defined absorption features at 1.22 eV, 1.66 eV, and 2.14 eV, which were assigned to charge-transfer excitons and in-gap defect states probably related to oxygen vacancies. More experiments are underway to gather a further insight into the phenomena observed in Fig. 5(b). All KNBF show Urbach tails; however, their appearance in optical absorption near band edges are expected in any material with disorder having a correlation length of order of the interatomic spacing, as this causes fluctuations in the electron energies $\sim(\text{eV})^2$.

Crystal chemistry arguments can be recalled to partially explain bandgap narrowing in KNBF as follows: (i) the replacement of Nb^{5+} by Fe^{3+} creates underbonded O^{2-} adjacent to the Fe^{3+}, which form FeO_6 octahedra, (ii) Bi^{3+} which tend to be off-center, create short, strong Bi-O (covalent) bonds that partially compensate for the loss of B-O bonding, (iii) K^+ do not off-center and are less prone to compensate the decrease B-O bonding. As a result, the repulsion between the non-bonding O charge densities and Fe 3d states is relatively weak, leading to an upshift of the VBM, which is composed of O 2p and Fe 3d states. The lattice distortion decreases markedly with x increasing from 0 to 0.05 and remains small (i.e., below the resolution limit of X-ray diffraction) above this concentration, as shown in Fig. 1. Coincidentally, the bandgap narrowing is the greatest in this compositional range as shown in Fig. 5, and the A_1 (LO) and A_1(TO) modes exhibit the largest shift, as shown by the dashed lines in Fig. 2. Hence, the magnitude of distortion is expected to have a major effect on the bandgap, modifying both CBM and VBM. The exact effect will depend on the coupling between the lattice strain and atomic displacements, understanding of which obviously requires further studies.

In summary, it was demonstrated that the band gap of orthorhombic ferroelectric $KNbO_3$ can be systematically narrowed by 1 eV (i.e., a ~33% reduction) via co-substitution of K and Nb by Bi and Fe, respectively. Remarkably, this bandgap narrowing is achieved while maintaining long-range polar order over a wide temperature range.

C.P.G. acknowledges SHU for a VC doctoral scholarship. Ian M. Reaney acknowledges the support from the Engineering and Physical Sciences Research Council through EP/L017563/1.

[1]A. Bhatnagar, A. R. Chaudhuri, Y. H. Kim, D. Hesse, and M. Alexe, Nature Commun. **4**, 2835 (2013).
[2]B. Kundys, Appl. Phys. Rev. **2**(1), 011301 (2015).
[3]L. P. Avakyants and D. F. Kiselev, Fiz. Tverd. Tela **20**(2), 611 (1978).
[4]Y. F. Cui, J. Briscoe, and S. Dunn, Chem. Mater. **25**(21), 4215 (2013).
[5]C. M. Hung, C. S. Tu, W. D. Yen, L. S. Jou, M. D. Jiang, and V. H. Schmidt, J. Appl. Phys. **111**(7), 07D912 (2012).
[6]I. Grinberg, D. V. West, M. Torres, G. Y. Gou, D. M. Stein, L. Y. Wu, G. N. Chen, E. M. Gallo, A. R. Akbashev, P. K. Davies, J. E. Spanier, and A. M. Rappe, Nature **503**(7477), 509 (2013).
[7]R. Agarwal, Y. Sharma, and R. S. Katiyar, Appl. Phys. Lett. **107**(16), 162904 (2015).
[8]R. K. Katiyar, Y. Sharma, D. Barrionuevo, S. Kooriyattil, S. P. Pavunny, J. S. Young, G. Morell, B. R. Weiner, R. S. Katiyar, and J. F. Scott, Appl. Phys. Lett. **106**(8), 082903 (2015).
[9]C. Pascual-Gonzalez, G. Schileo, and A. Feteira, Appl. Phys. Lett. **109**(13), 132902 (2016).
[10]L. M. Yu, J. H. Jia, G. W. Yi, Y. Shan, and M. M. Han, Mater. Lett. **184**, 166 (2016).
[11]G. Shirane, H. Danner, A. Pavlovic, and R. Pepinsky, Phys. Rev. **93**(4), 672 (1954).
[12]F. G. Wang, I. Grinberg, and A. M. Rappe, Phys. Rev. B **89**(23), 235105 (2014).
[13]Y. P. Guo, B. Guo, W. Dong, H. Li, and H. Z. Liu, Nanotechnology **24**(27), 275201 (2013).
[14]A. M. Quittet, M. I. Bell, M. Krauzman, and P. M. Raccah, Phys. Rev. B **14**(11), 5068 (1976).
[15]L. Luisman, A. Feteira, and K. Reichmann, Appl. Phys. Lett. **99**(19), 192901 (2011).
[16]V. Krayzman, I. Levin, J. C. Woicik, and F. Bridges, Appl. Phys. Lett. **107**(19), 192903 (2015).
[17]C. Pascual-Gonzalez, G. Schileo, A. Khesro, I. Sterianou, D. Wang, I. M. Reaney, and A. Feteira, J. Mater. Chem. C **5**(8), 1990 (2017).
[18]F. Burkert, J. Kreisel, and C. A. Kuntscher, Appl. Phys. Lett. **109**(18), 182903 (2016).